Electronic Supplementary Information (ESI)

Realization of robust mesoscale ionic diodes for ultrahigh osmotic energy generation at mild neutral pH

Pei-Ching Tsai,[1,+] Yen-Shao Su,[1,+] Mengyao Gao,[1] Li-Hsien Yeh,[1,*]

[1]Department of Chemical Engineering, National Taiwan University of Science and Technology, Taipei 10607, Taiwan

[*] Corresponding Author:

E-mail: lhyeh@mail.ntust.edu.tw, TEL: +886-2-27376942 (Li-Hsien Yeh)

+ These two authors contributed equally to this work

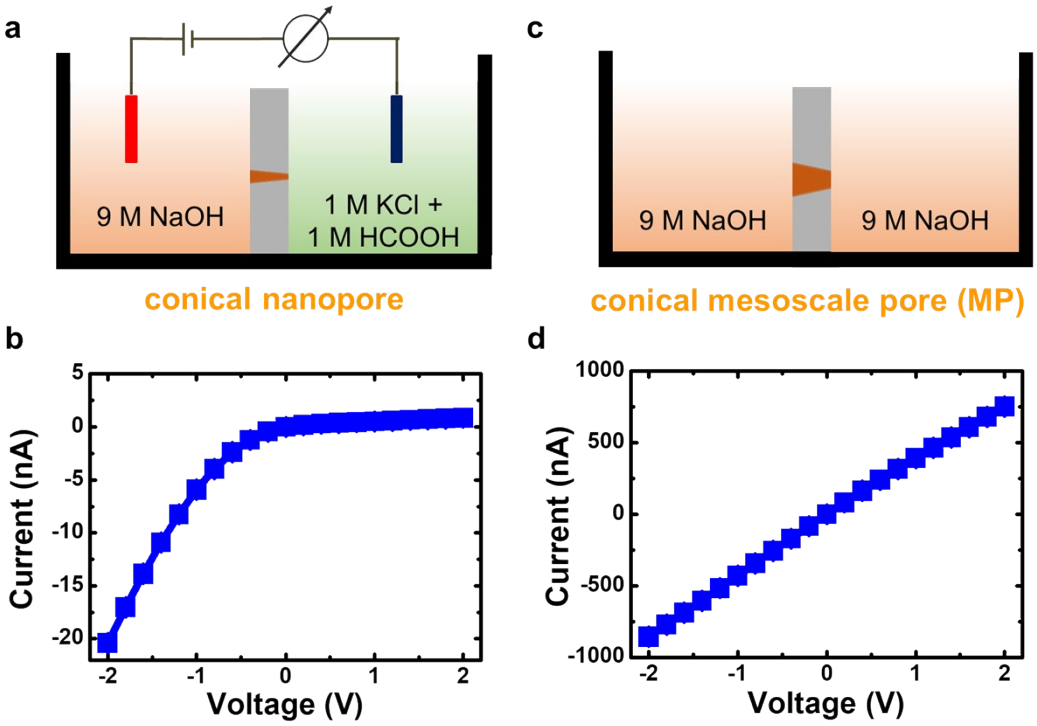

Fig. S1. Fabrication of a single conical mesoscale pore (MP). (a) Pre-fabrication of a single conical nanopore by the asymmetric track-etching technique and (b) its I-V response in 100 mM KCl solution, which showed apparent ICR effect. The tip diameter of the as-prepared nanopore in (b) was ~4 nm. (c) Fabrication of a single conical MP through a pore widening process in symmetric 9 M NaOH solutions and (d) its I-V response in 100 mM KCl solution, which showed linear Ohmic behavior because the electric double layers in the pore are no longer overlapped. The tip diameter of the fabricated MP in (d) was ~700 nm.

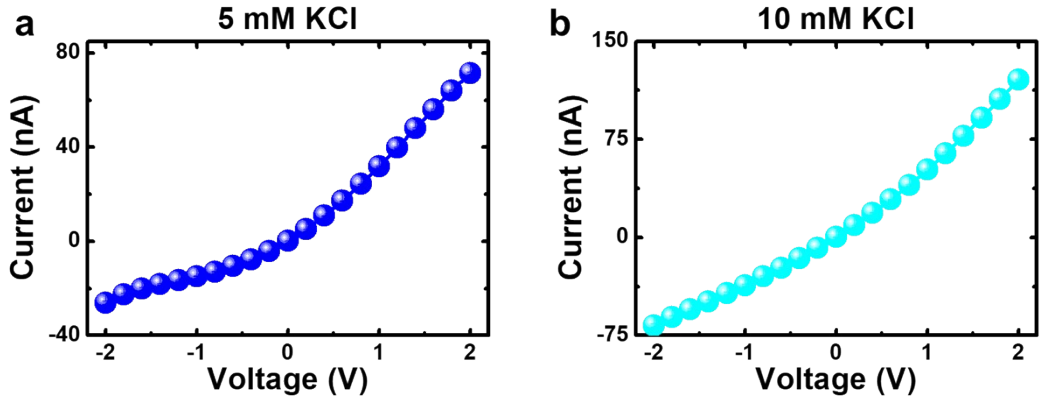

Fig. S2. I-V curves of the single PLL-functionalized conical MP with tip diameter of ~700 nm measured in (a) 5 mM and (b) 10 mM KCl solutions at neutral pH. The pore membrane is the same as that used in Fig. 2.

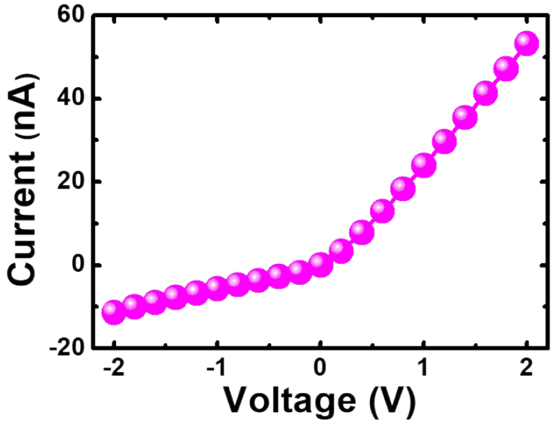

Fig. S3. I-V curve of a single PLL-functionalized conical MP with tip diameter of ~800 nm measured in 1 mM KCl solution at neutral pH. The pore membrane is the same as that used in Fig. 3 and the measurement was conducted after it was stored in ambient environment at room temperature for two weeks.

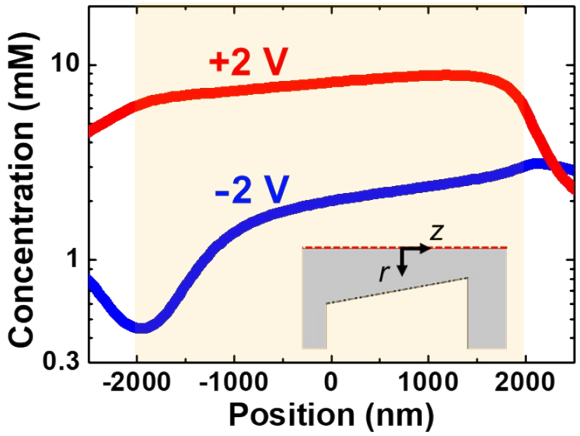

Fig. S4. Axial variations of the cross-sectionally averaged total ionic concentration in the polyelectrolyte (PE) functionalized conical MP at the two applied voltages with opposite signs. The simulation parameters are the same as those in Fig. 4d.

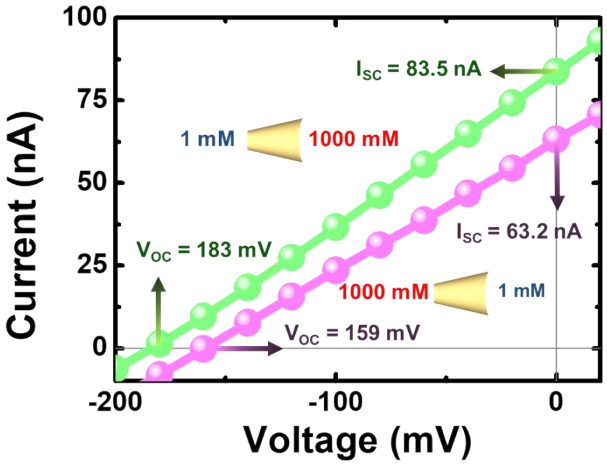

Fig. S5. I-V curves of a single PLL-functionalized MP with tip diameter of ~700 nm recorded under two configurations of a 1000-fold KCl gradient at mild neutral pH. The V_{OC} and I_{SC} increase by about 15 and 32 %, respectively, when the base opening of the pore faces the concentrated solution.

Electrode calibration with redox potential

The pure concentration gradient-driven osmotic energy conversion of the mesoscale ionic diode considered was determined by scanning I-V curves under different KCl gradients. The sweeping voltages varying from –0.2 to 0.2 V with a step of 0.02 V were applied on the electrode in the cell facing the base side of the membrane. Under a concentration gradient, the measured open-circuit voltage (V_{oc}) of an ion-selective pore includes two parts, one of which is the redox potential (V_{red}) resulting from the uneven voltage drop on the electrodes and the other is the osmotic voltage (V_{osm}) contributed by the pure concentration gradient (Fig. S6).[1] Consequently, the pure concentration gradient-driven osmotic voltage was determined by

$$V_{osm} = V_{oc} - V_{red} \tag{S1}$$

In this study, the values of V_{red} at various KCl gradients were estimated by measuring the potential difference of the bare un-modified MP membrane that is expected to be non-ion-selective using the same conductive cells (Fig. S7 and Table S1). The electrode calibration method adopted has been widely used for identifying osmotic energy conversion performance in single-pore systems.[1]

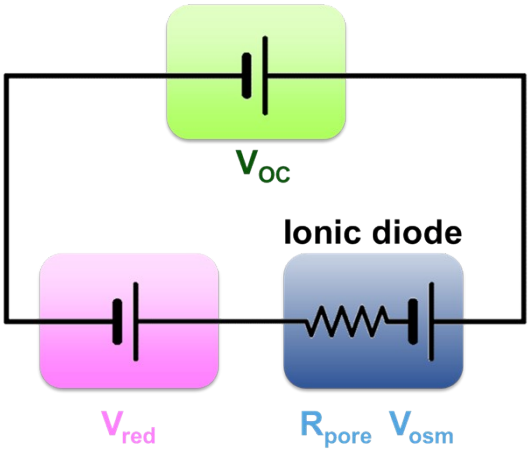

Fig. S6. Equivalent circuit of the mesoscale ionic diode system under consideration.

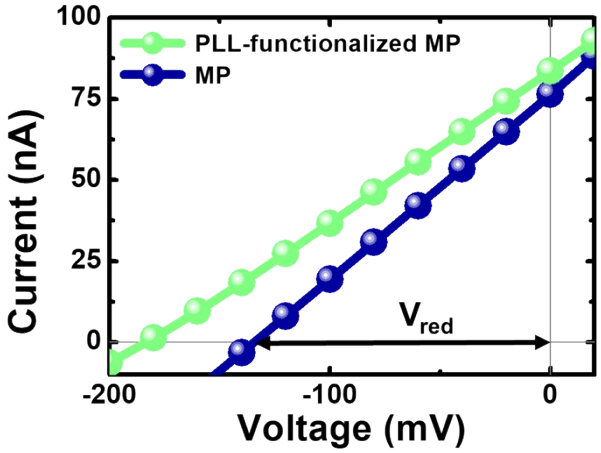

Fig. S7. I-V curves of a single conical MP with tip diameter of ~700 nm before (blue solid line with circles) and after (green solid line with circles) PLL functionalization recorded under a 1000-fold KCl gradient at mild neutral pH. The redox potential (V_{red}) can be obtained from the voltage intercept of the un-modified bare MP which is non-ion-selective.

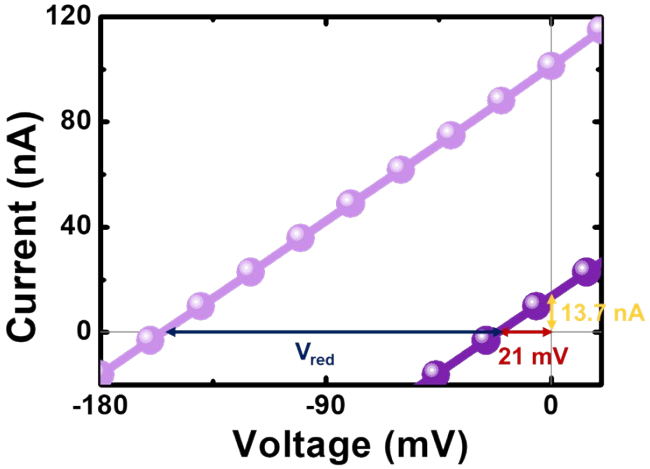

Fig. S8. I-V curves of a single PLL-functionalized pore with tip diameter of ~1000 nm tested under a 1000-fold KCl gradient at mild neutral pH. The light and dark purple curves represent the results before and after the electrode calibration with V_{red}, respectively. The realized V_{osm} and I_{osm} are about 21.0 mV and 13.7 nA, respectively, achieving a maximum osmotic power of ~71.9 pW.

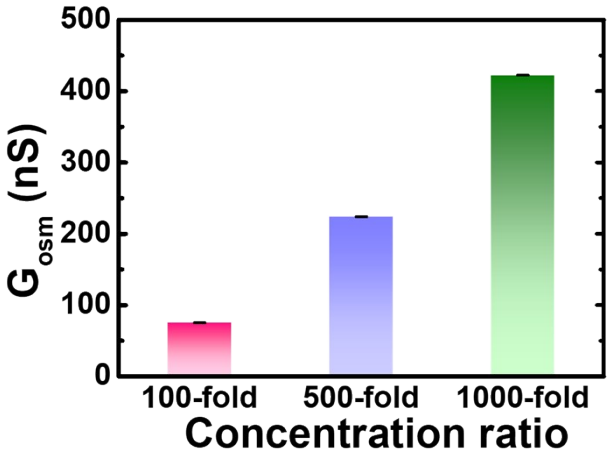

Fig. S9. Osmotic conductance (G_{osm}) of the exploited mesoscale ionic diode as a function of KCl gradient measured at mild neutral pH condition. The is the same pore membrane used in Fig. 5.

Table S1. Summary of the averaged values of the redox potential (V_{red}), open-circuit voltage (V_{oc}), short-circuit current (I_{sc}), osmotic current (I_{osm}), osmotic voltage (V_{osm}), osmotic conductance (G_{osm}) and osmotic power (P_{osm}) generated from the present mesoscale ionic diode system as a function of KCl gradient. All measurements were performed under neutral pH condition.

KCl gradient (mM/mM)	V_{red} (mV)	V_{oc} (mV)	I_{sc} (nA)	V_{osm} (mV)	I_{osm} (nA)	G_{osm} (nS)	P_{osm} (pW)
100/1	103	111	8.06	8.00	0.603	75.4	1.21
500/1	118	146	34.9	28.0	6.27	224	43.9
1000/1	134	183	83.5	49.0	20.7	423	254

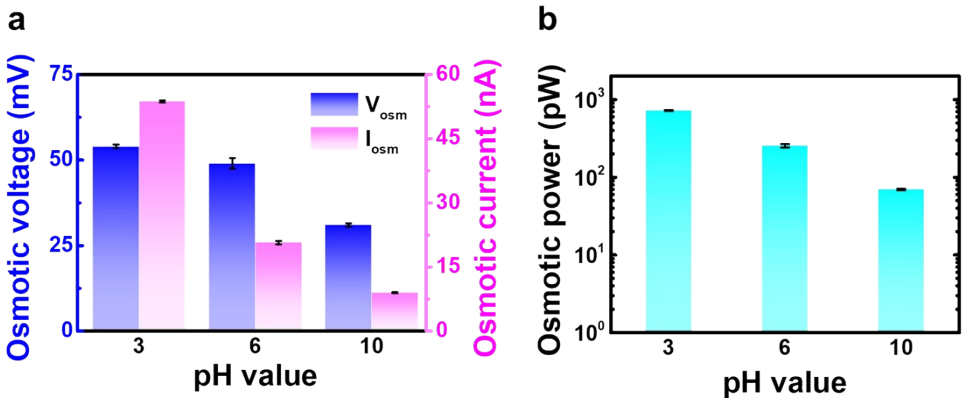

Fig. S10. The pH effect on the (a) osmotic voltage, osmotic current and (b) osmotic power generated by the exploited mesoscale ionic diode. The tip pore size is about 700 nm and the salinity gradient is fixed at 1000 mM/1 mM KCl.

Table S2. Summary of the averaged values of V_{oc}, I_{sc}, V_{red}, V_{osm}, I_{osm}, and P_{osm} generated from the present mesoscale ionic diode system in acidic (pH 3) and basic (pH 10) environments. All measurements were performed under a 1000 mM/1 mM KCl gradient.

pH	V_{oc} (mV)	I_{sc} (nA)	V_{red} (mV)	V_{osm} (mV)	I_{osm} (nA)	P_{osm} (pW)
3	188	220	134	54.0	53.7	725
10	165	54.4	134	31.0	8.99	69.7

Table S3. Comparison of the osmotic power generated from the earlier state-of-the-art single nanopore-based devices with various pore sizes reported in the literatures and the present mesoscale ionic diode system. All the data were conducted under mild neutral pH condition.

Single-pore	Size (nm)	pH	Osmotic power (pW)	Ref.
hBN nanotube	80	Neutral	0.934	[1]
PI conical nanopore	72	Neutral	26	[2]
PI conical nanochannel	40	Neutral	45	[3]
MoS_2 nanopore	3	Neutral	9.51	[4]
PE-modified nanopore	14	Neutral	25	[5]
Gel-functionalized nanopore	70	Neutral	20	[6]
Light-enhanced MoS_2 nanopore	10	Neutral	40.2	[7]
Bullet-shaped nanopore	30	Neutral	45	[8]
PLL-functionalized MP	700	Neutral	254	This work

Table S4. Comparison of the osmotic power generated from the present work with the earlier reported state-of-the-art single nanopore-based devices, which were operated in high basic or acidic solutions.

Single-pore	Size (nm)	pH	Osmotic power (pW)	Ref.
PLL-functionalized MP	700	Neutral	254	This work
hBN nanotube	80	11	20	[1]
MoS_2 nanopore	11.2	11	232	[4]
Bullet-shaped nanopore	30	10	80	[8]
PANI-coated nanopore	70	3.5	15	[9]

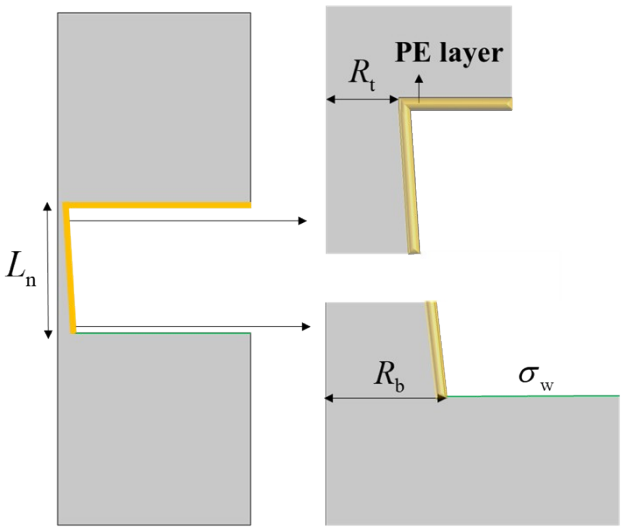

Fig. S11. Schematic of the simulated MP system where the inner wall of a MP and the upper wall of the pore membrane cover a homogeneous PE layer carrying high space charge density, and the lower wall of the pore membrane bears the original surface charge density of σ_w.

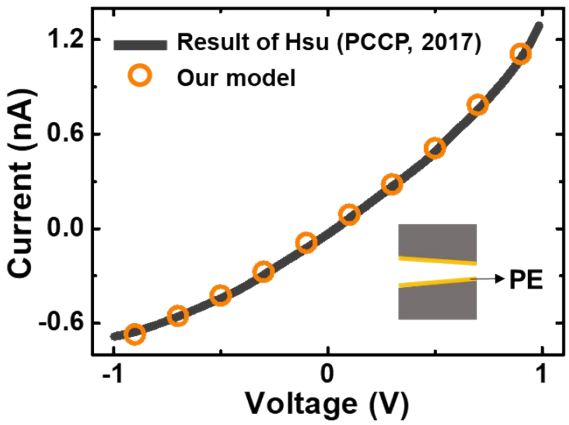

Fig. S12. The validation of the continuum model we adopted. Solid curve denotes the result of Hsu et al.,[10] who examined the I-V curve of a PE-coated conical nanopore with tip size of 20 nm, base size of 196 nm, and a PE layer of 5 nm in thickness and -1.12×10^{7} C/m^{3} in space charge density at 10 mM KCl. Circles denote our modeling results. The prediction from our model agrees well with the result of Hsu et al.,[10] demonstrating the applicability of our model.

Numerical Simulation

The PE functionalized conical MP system considered is schematically depicted in Fig. S11. A PE layer carrying a high space charge density of ρ_{PE} is covered entirely on the upper wall of the pore membrane and the inner wall of a solid-state conical MP with tip radius of R_t, base radius of R_b and length of L_n. Two large and identical reservoirs are connected to the MP, and a binary electrolyte aqueous solution (*i.e.*, KCl solution) is filled with the entire simulation system. Suppose that the PE layer is ion-penetrable, homogeneously structured and of uniform thickness l_{PE}. The ion transport property in a PE functionalized MP can be described by the following coupled Poisson-Nernst-Planck and Stokes-Brinkman equations with considering the space charge density stemming from the PE layer,[11, 12]

$$-\nabla^2\phi = \frac{h\rho_{\mathrm{PE}} + \sum_{i=1}^{2} Fz_iC_i}{\varepsilon_f} \tag{S2}$$

$$\nabla\cdot\mathbf{J}_i = \nabla\cdot\left(\mathbf{u}C_i - D_i\nabla C_i - z_i\frac{D_i}{RT}FC_i\nabla\phi\right) = 0,\ i = 1, 2 \tag{S3}$$

$$\mu\nabla^2\mathbf{u} - \nabla p - \left(\sum_{i=1}^{2} Fz_iC_i\right)\nabla\phi - h\frac{\mu}{(\lambda_{PE})^2}\mathbf{u} = 0 \tag{S4}$$

$$\nabla\cdot\mathbf{u} = 0 \tag{S5}$$

In the above, ϕ is the electrical potential; F, R, and T are the Faraday constant, gas constant, and fluid temperature, respectively; ε_f, $\mathbf{u}$, p, and μ are the permittivity, velocity, pressure and dynamic viscosity of fluid, respectively; z_i, C_i, $\mathbf{J}_i$, and D_i are the valence, concentration, flux, and diffusivity of the ionic species of i ($i = 1$ for $\mathrm{K^+}$ ions and $i = 2$ for $\mathrm{Cl^-}$ ions); h is the region function ($h = 1$ denotes the region inside the PE layer and $h = 0$ denotes the region outside the PE layer); $\lambda_{PE} = (\mu/\gamma_{PE})^2$ is the softness degree of the PE layer with γ_{PE} being the hydrodynamic frictional coefficient of this layer. For simplicity, we

assume $\lambda_{PE} = 1$ nm, in accordance with the typical value of artificial PEs (ca. 0.1-10 nm).[13]

To simulate the experimental setup, we assume the following boundary conditions. (i) The end of the reservoir outside the base-side MP is applied at a voltage bias V (*i.e.*, $\phi = V$), while the end of the reservoir outside the tip-side MP is grounded (*i.e.*, $\phi = 0$). (ii) The ionic concentrations at the ends of two reservoirs reach the bulk concentration of electrolyte (*i.e.*, $C_i = C_{\mathrm{KCl}}$ or $C_i = C_h$ and $C_i = C_l$) and there is no applied pressure gradient through the system (*i.e.*, $p = 0$). (iii) The rigid walls of the inner MP and the upper pore membrane are non-slip ($\mathbf{u} = 0$), ion-impenetrable ($\mathbf{n} \cdot \mathbf{J}_i = 0$), and carry free of surface charges ($\mathbf{n} \cdot \nabla\phi = 0$). Here **n** is the unit outer normal vector. The rigid wall of the lower pore membrane is non-slip ($\mathbf{u} = 0$), ion-impenetrable ($\mathbf{n} \cdot \mathbf{J}_i = 0$), and carry a surface charge density of σ_w ($-\varepsilon_f \mathbf{n} \cdot \nabla\phi = \sigma_w$). In the modeling, we assume $\sigma_w = -40$ mC/m^2, corresponding to the value of the etched PET pore membrane at about pH 6.[14] (iv) The electric potential, electric field, ionic concentrations, and flow field are all continuous on the PE layer/liquid interfaces. (v) The symmetric boundary condition is specified along the axis of the MP.

When a voltage bias is applied through the system, the ionic current through the pore can be estimated as

$$I = \int_S F(\sum_{i=1}^{2} z_i \mathbf{J}_i) \cdot \mathbf{n} \, dS, \tag{S6}$$

where *S* denotes either end of the reservoirs. The parameters we used for the PE modified MP system include $R_t = 350$ nm, $R_b = 650$ nm, $L_n = 4000$ nm, and $l_{PE} = 10$ nm.

4. References

1. A. Siria, P. Poncharal, A. L. Biance, R. Fulcrand, X. Blase, S. T. Purcell and L. Bocquet, *Nature*, 2013, **494**, 455-458.
2. W. Guo, L. Cao, J. Xia, F.-Q. Nie, W. Ma, J. Xue, Y. Song, D. Zhu, Y. Wang and L. Jiang, *Advanced Functional Materials*, 2010, **20**, 1339-1344.
3. L. X. Cao, W. Guo, W. Ma, L. Wang, F. Xia, S. T. Wang, Y. G. Wang, L. Jiang and D. B. Zhu, *Energy Environ. Sci.*, 2011, **4**, 2259-2266.
4. J. D. Feng, M. Graf, K. Liu, D. Ovchinnikov, D. Dumcenco, M. Heiranian, V. Nandigana, N. R. Aluru, A. Kis and A. Radenovic, *Nature*, 2016, **536**, 197-200.
5. S. Balme, T. J. Ma, E. Balanzat and J. M. Janot, *J. Membr. Sci.*, 2017, **544**, 18-24.
6. T. J. Ma, E. Balanzat, J. M. Janot and S. Balme, *ACS Appl. Mater. Interfaces*, 2019, **11**, 12578-12585.
7. M. Graf, M. Lihter, D. Unuchek, A. Sarathy, J. P. Leburton, A. Kis and A. Radenovic, *Joule*, 2019, **3**, 1549-1564.
8. G. Laucirica, A. G. Albesa, M. E. Toimil-Molares, C. Trautmann, W. A. Marmisolle and O. Azzaroni, *Nano Energy*, 2020, **71**, 104612.
9. G. Laucirica, M. E. Toimil-Molares, C. Trautmann, W. Marmisoll and O. Azzaroni, *ACS Appl. Mater. Interfaces*, 2020, **12**, 28148-28157.
10. J. P. Hsu, H. H. Wu, C. Y. Lin and S. Tseng, *Phys. Chem. Chem. Phys.*, 2017, **19**, 5351-5360.
11. L. H. Yeh, M. Zhang, N. Hu, S. W. Joo, S. Qian and J. P. Hsu, *Nanoscale*, 2012, **4**, 5169-5177.
12. C. Y. Lin, J. P. Hsu and L. H. Yeh, *Sens. Actuator B-Chem.*, 2018, **258**, 1223-1229.
13. Z. Zeng, L. H. Yeh, M. Zhang and S. Qian, *Nanoscale*, 2015, **7**, 17020-17029.
14. C. Y. Lin, L. H. Yeh and Z. S. Siwy, *J. Phys. Chem. Lett.*, 2018, **9**, 393-398.